Heavy Nondegenerate Electrons in Doped Strontium Titanate

Clément Collignon, Phillipe Bourges, Benoît Fauqué, Kamran Behnia

Heavy Nondegenerate Electrons in Doped Strontium Titanate

Clément Collignon,[1,2,*] Phillipe Bourges,[3] Benoît Fauqué,[1,†] and Kamran Behnia[2]

[1]*JEIP, USR 3573 CNRS, Collège de France, PSL University, 11, place Marcelin Berthelot, 75231 Paris Cedex 05, France*

[2]*Laboratoire Physique et Etude de Matériaux (CNRS-Sorbonne Université), ESPCI, PSL Research University, 75005, Paris, France*

[3]*Laboratoire Léon Brillouin, CEA-CNRS, Université Paris-Saclay, CEA Saclay, 91191 Gif-sur-Yvette, France*

(Received 14 January 2020; revised 17 April 2020; accepted 28 May 2020; published 3 August 2020)

Room-temperature metallicity of lightly doped $SrTiO_3$ is puzzling, because the combination of mobility and the effective mass would imply a mean-free path below the Mott-Ioffe-Regel limit and a scattering time shorter than the Planckian time ($\tau_P = \hbar/k_B T$). We present a study of electric resistivity, Seebeck coefficient, and inelastic neutron scattering extended to very high temperatures, which deepens the puzzle. Metallic resistivity persists up to 900 K and is accompanied by a large Seebeck coefficient whose magnitude (as well as its temperature and doping dependence) indicates that carriers are becoming heavier with rising temperature. Combining this with neutron scattering data, we find that between 500 and 900 K the Bohr radius and the electron wavelength become comparable to each other and twice the lattice parameter. According to our results, between 100 and 500 K, metallicity is partially driven by temperature-induced amplification of the carrier mass. We contrast this mass amplification of nondegenerate electrons with the better-known case of heavy degenerate electrons. Above 500 K, the mean-free path continues to shrink with warming in spite of becoming shorter than both the interatomic distance and the thermal wavelength of the electrons. The latter saturates to twice the lattice parameter. Available theories of polaronic quasiparticles do not provide satisfactory explanation for our observations.

DOI: 10.1103/PhysRevX.10.031025 Subject Areas: Condensed Matter Physics

I. INTRODUCTION

Decades ago [1], Mott argued that the threshold of metallicity in a doped semiconductor depends on the effective range of the Coulomb interaction exerted by an extrinsic atom, the Bohr radius. According to what is now known as the Mott criterion for metal-insulator transition [2,3], a semiconductor becomes metallic when the density of its carriers n exceeds a threshold set by its effective Bohr radius $a_B^\star$:

$$n^{1/3} a_B^\star > 0.25. \tag{1}$$

Since $a_B^\star = 4\pi\epsilon\hbar/m^\star e^2$ (where $m^\star$ is the mass carrier and ϵ the dielectric constant), a small $m^\star$ or a large ϵ would favor the emergence of metallicity at low doping.

Strontium titanate is a wide-gap semiconductor whose electric permittivity becomes as large as 20 000 times the vacuum permittivity in liquid helium temperature [4–7], which implies a Bohr radius approaching a micron [8]. As a consequence, one can easily turn it to a metal [9] with one carrier per 10^5 unit cells. This dilute metal has attracted renewed attention in recent years for multiple reasons [10]. First of all, it becomes a superconductor [11], implying that Cooper pairs can be formed even when the Fermi energy is an order of magnitude lower than the Debye energy [12–18]. The dilute superconductor [19,20] appears to be intimately linked to aborted ferroelectricity [21–26]. Second, the high mobility of carriers at low temperature allows the observation of quantum oscillations [12,27–29] in relatively low magnetic fields. The evolution of the Fermi surface with doping can be explored and compared with what is expected by theory [30], and test the limits of rigid-band approximation. Third, the low-temperature resistivity displays a quadratic temperature dependence [30–35] with a prefactor which smoothly increases with decreasing carrier concentration [32]. Such a T-square resistivity is expected in a Fermi liquid with dominant e^--e^- scattering. However, here, the behavior persists even in the extreme dilute limit in the absence of umklapp

*Present address: Department of Physics, Massachusetts Institute of Technology, Cambridge, Massachusetts 02139, USA.

†benoit.fauque@espci.fr

scattering [32]. Finally, the high-temperature metallicity is "beyond quasiparticles" [36–38]. The combination of room-temperature resistivity and low-temperature effective mass implies a mean-free path that falls below all known length scales of the solid (the electron wavelength and the lattice parameter) [36]. This has been observed in strange metals with strong correlation among electrons [39], in organic semiconductors [40], but not in inorganic doped band insulators.

In this paper, we address this last issue by measuring the resistivity and the Seebeck coefficient of $SrTi_{1-x}Nb_xO_3$ up to temperatures as high as 900 K, in which, in contrast to oxygen-reduced strontium titanate, exposition to high temperatures does not modify the number of dopants (see Sec. V). We find that even at 900 K, resistivity continues to increase and the Seebeck data imply that electron mass evolves as a function of temperature. We also present a study of inelastic neutron scattering, which documents the evolution of the soft zone center transverse optical (TO) phonon mode above room temperature. After presenting our resistivity data, we demonstrate the features shared by metallic strontium titanate with other systems close to a ferroelectric instability in contrast to ordinary metallic (i.e., "heavily doped" [41]) semiconductors. We will see that the magnitude of mobility combined with low-temperature effective mass would imply a scattering time shorter than the Planckian time, a feature which would distinguish this metal from other "strange" metals, which respect this limit [42]. Then we present our Seebeck data and argue that the expression for the thermoelectric response of nondegenerate electrons [43] implies a temperature-induced amplification of the carrier mass. The extracted heavy masses shift upward the temperature window where the scattering time falls below the Planckian time. The amplified mass combined with the dielectric permittivity extracted from the neutron data allows us to conclude that for $T > 500$ K, the Bohr radius and the thermal wavelength both shrink to twice the lattice parameter and much shorter than the interelectron distance. The persistence of metallicity in this context remains beyond any available quasiparticle-based picture and is a new challenge to theory, which has started to tackle charge transport in dilute metallic strontium titanate [37,38].

One conclusion is that in this metal, the temperature dependence of resistivity is partially set by the evolution of the effective mass. This idea was previously put forward by Eagles *et al.*, who invoked "mixed polarons" [44]. Nevertheless, we argue that the underlying microscopic interaction is yet to be identified.

II. RESULTS

A. Resistivity of doped strontium titanate from 2 to 900 K

Figure 1(a) shows the temperature dependence of resistivity for six niobium-doped samples with carrier concentrations ranging from 1.4×10^{18} to $3.5\times10^{20}\,\mathrm{cm}^{-3}$. Our data below 300 K are in agreement with previous old [45–47] and recent [9,32,33,36,48] studies of charge transport in this system (see Ref. [10] for a review). Let us note that reproducible measurements at high temperatures are challenging, because of the possible variation in the number of oxygen vacancies with increasing temperature. Our measurements were performed in the presence of adequate air pressure. Frederikse and Hosler [46] checked that the Hall number n_H of Nb-doped strontium titanate remains temperature independent up to 1000 K.

As one can see in Fig. 1, the metallic resistivity, problematic even at room temperature [36], persists up to 900 K. Figure 1(b) displays the temperature dependence of mobility. Upon warming, it changes by 4 orders of magnitude. The room-temperature mobility is as low as 5 $\mathrm{cm}^2/\mathrm{V\,s}$. As we will see below, this is uncommonly small among metallic semiconductors. Upon warming to 900 K, it falls below 1 $\mathrm{cm}^2/\mathrm{V\,s}$. As shown in the inset of Fig. 1, at 900 K, with a 100-fold increase of carrier concentration, mobility slightly decreases from 0.7 to 0.5 $\mathrm{cm}^2/\mathrm{V\,s}$. At room temperature, it does not display any detectable

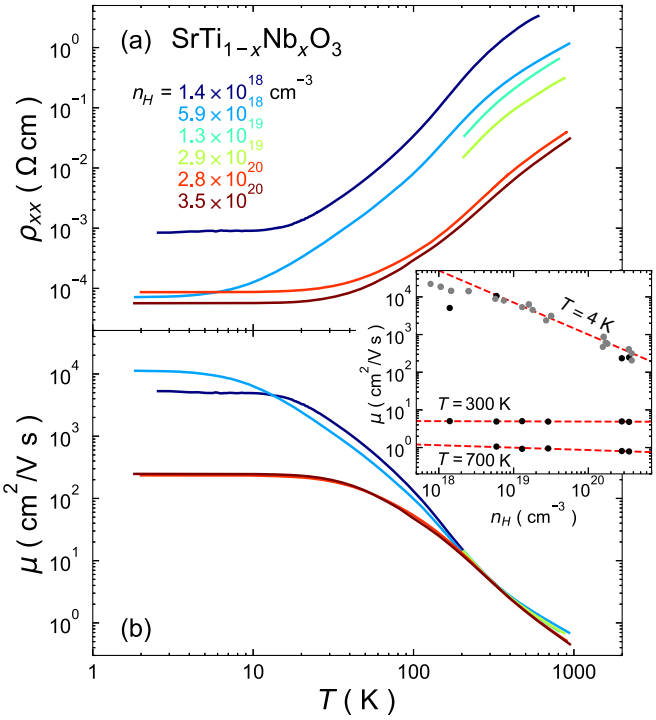

FIG. 1. (a) Temperature dependency of the resistivity extended to 900 K for several Nb-doped $SrTiO_3$ crystals. The metallic behavior continues up to 900 K. (b) Temperature dependency of the Hall mobility $\mu = 1/(\rho n_H e)$ from 2 to 900 K of the same samples. The inset shows the dependence of mobility on carrier concentration at different temperatures. At room temperature and above, the mobility is low and shows little variation with carrier concentration. At low temperatures, the mobility is large and strongly depends on carrier concentration.

dependence on carrier concentration. In contrast, at low temperature, when impurity scattering dominates, it becomes orders of magnitude larger and shows a strong dependence on carrier density. As we will see below, the presence or absence of these features distinguishes two groups of dilute metals.

B. Mean-free path and scattering time

As previously noticed [36], the measured mobility of $\mu = 4.9 \pm 0.5$ cm^2/V s at $T = 300$ K implies a mean-free path falling below any relevant length scale of the system. Since the mobility becomes almost an order of magnitude smaller at 900 K, the breakdown of the quasiparticle picture is becoming more drastic. This can be seen in Fig. 2(a),

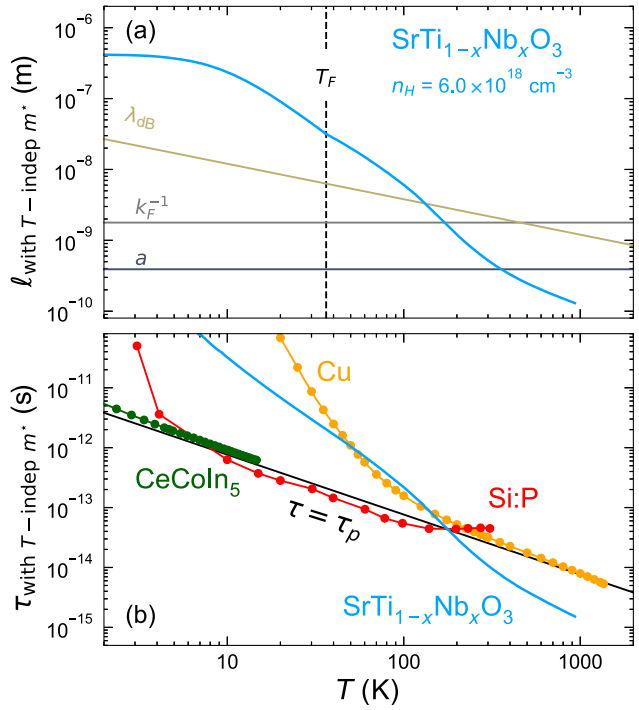

FIG. 2. (a) Temperature dependency of the mean-free path ℓ of Nb-doped $SrTiO_3$ for $n_H = 5.9\times10^{18}$ cm^{-3}, using the low-temperature effective mass. The lattice parameter a, the inverse of Fermi wave vector k_F^{-1}, and the de Broglie thermal wavelength λ_{dB} are also plotted. ℓ is computed using Eq. (2) when $T < T_F$ and using Eq. (3) when $T > T_F$. The mass used to compute ℓ and λ_{dB} is the one measured at low temperature through quantum oscillations [28]. (b) Temperature dependency of the inelastic scattering time, $\tau = m^\star/ne^2(\rho-\rho_0)$, of the same sample. Also shown are the inelastic scattering time of P-doped Si (a doped semiconductor), copper (a good metal), and $CeCoIn_5$ (a bad metal). The Planckian time $\hbar/k_BT$ is also plotted in black. Except for Nb-doped $SrTiO_3$, the scattering time in all cases remains longer than the Planckian time. Note that electrons in Cu and in $CeCoIn_5$ remain degenerate, but in P-doped Si and Nb-doped $SrTiO_3$ they become non-degenerate above 60 and 40 K, respectively. The resistivity and the effective mass data for Si, Cu, and $CeCoIn_5$ are taken from Refs. [49–55].

which shows the temperature dependence of the mean-free path of the sample with $n_H = 5.9\times10^{18}$ cm^{-3}. Also plotted are the inverse Fermi wave vector k_F^{-1}, the lattice parameter a, and the de Broglie wavelength $\lambda_{dB} = \sqrt{2\pi\hbar^2/m^\star k_BT}$.

Below the degeneracy temperature, $T_F = 39$ K, the velocity of electrons is $v_F = \hbar k_F/m^\star$. Therefore, assuming a simple Drude law, $\sigma = ne^2\tau/m^\star$, and by noting that $\ell = v_F\tau$ and $k_F^3 = 3\pi^2 n$, we get a mass independent mean-free path:

$$\ell_{T<T_F} = \frac{\mu}{e}\hbar k_F = \frac{\mu}{e}\hbar(3\pi^2 n)^{1/3}, \tag{2}$$

where ρ is the resistivity and n the carrier concentration.

Above T_F, electrons become nondegenerate and the velocity of carriers is not the Fermi velocity but the thermal velocity $v_{th} = \sqrt{2k_BT/m^\star}$. The scattering time can be extracted from resistivity, assuming once again a simple Drude law and $\ell = v_{th}\tau$:

$$\ell_{T>T_F} = (2\sqrt{\pi})\frac{\mu}{e}\hbar\lambda_{dB}^{-1} = \frac{\mu}{e}\sqrt{2m^\star k_BT}. \tag{3}$$

Note that in both cases mobility is simply the ratio of the mean-free path to momentum. The only difference is that this momentum is the Fermi momentum below T_F and the thermal momentum above. According to Eq. (2), one needs the effective mass to quantify λ_{dB} and ℓ in the nondegenerate regime. In Fig. 2, it has been assumed that $m^\star \simeq 3.8m_e$, which is the heaviest cyclotron mass detected by quantum oscillations at low temperatures [28]. Taking a lighter mass would shorten further the mean-free path. The figure shows that at 900 K, the mean-free path becomes 4 times shorter than the interlattice spacing and one order of magnitude below λ_{dB}.

The so-called Mott-Ioffe-Regel (MIR) limit [56,57] is a lower boundary to the mean-free path of carriers of a metal. This minimum length is either the lattice parameter or the quasiparticle wavelength [58]. Most metals respect this limit and their resistivity saturates when the mean-free path becomes too short [59,60]. Metals which do not respect this limit [61,62] were dubbed bad metals [58]. Bruin *et al.* [42] noticed that good and bad metals both show a scattering time which does not fall below the Planckian time ($\tau_p = \hbar/k_BT$). This led to a theoretical proposal for the existence of such a bound to diffusive transport based on Heisenberg uncertainty [63].

The scattering time τ of our system can be easily quantified. It is the velocity (thermal above T_F and Fermi below) divided by the mean-free path. As seen in the lower panel of Fig. 2, at 900 K, τ falls one order of magnitude below τ_p. For comparison, we computed the inelastic scattering time of a good metal (pure Cu), a bad metal ($CeCoIn_5$), and a doped semiconductor

(P-doped Si) using their resistivity and effective mass, $\tau = m^\star/ne^2(\rho - \rho_0)$, extracted from published data [49–55]. As seen in the figure, their scattering time does not become shorter than the Planckian time as noticed by Bruin *et al.* [42].

At this stage, doped strontium titanate appears to behave remarkably bad, worse than cuprates, the most notorious of bad metals, which have been shown to obey the Planckian bound [64], even though they do not respect the MIR limit [61,62].

C. Two distinct types of dilute metals

It is surprising to find such a strangeness in what is, after all, merely a doped band insulator. Let us compare our system to other doped semiconductors. The origin of the absurdly short scattering time of strontium titanate is the large temperature dependence of mobility. It changes by 4 orders of magnitude between 900 and 2 K [see Fig. 1(b)]. Moreover, the 2 K mobility varies by a factor of 200 between $n_H = 6 \times 10^{18}$ and 3×10^{20} cm^{-3} (see the inset of Fig. 1).

Neither of these two features can be seen in ordinary semiconductors. In metallic phosphorous-doped silicon [49], in Sn-doped indium oxide (ITO) [65], and in doped ZnO [66–68], mobility displays little change with temperature and a modest decrease with the increase in carrier concentration (see Fig. 3). On the other hand, other polar semiconductors, which are close to a ferroelectric instability, such as IV-VI semiconductors (PbTe and PbSe) and ABO_3 perovskites (like $KTaO_3$ and $EuTiO_3$) display the two features seen in doped strontium titanate. Specifically, in these systems, mobility enhances by orders of magnitude upon cooling, and in cryogenic temperatures, displays a power-law dependence on carrier concentration (see Fig. 3). It has been argued [8] that the latter feature is an expected consequence of a Bohr radius exceeding by far the interatomic distance.

Like strontium titanate, these solids are quantum paraelectrics with soft phonons. However, since their room-temperature mobility is larger than strontium titanate, their mean-free path and their scattering time remain reasonably long. Nevertheless, the qualitative similarity seen among these dilute metals and the contrast with ordinary doped semiconductors suggest that the presence of a soft ferroelectric mode plays a role in the peculiar metallicity of doped strontium titanate.

D. High-temperature Seebeck coefficient

The temperature dependence of the Seebeck coefficient for five Nb doped $SrTiO_3$ samples between 10 and 800 K is shown in Fig. 4(a). Our data are in reasonable agreement with previous reports below room temperature 12,48,72]]. Lin *et al.* [12] reported that the Seebeck coefficient is T linear at low temperature as expected for

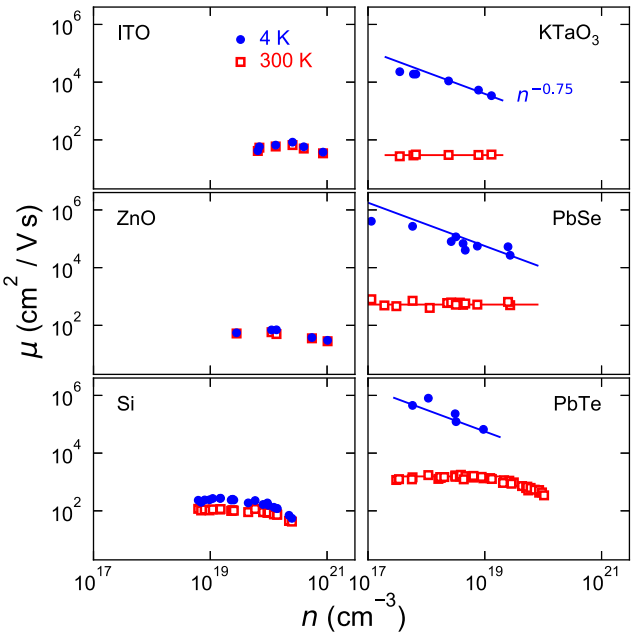

FIG. 3. Mobility as a function of doping at $T = 4$ K (full circles) and $T = 300$ K (open squares) in different dilute metals. Left-hand panels show the data for tin-doped In_2O_3 (ITO), Al- and Ga-doped ZnO, and phosphorus-doped silicon [49,65–68]. Right-hand panels show the data for $KTaO_3$, PbTe, and PbSe [69–71], which are all polar semiconductors close to a ferroelectric instability. In the first case, mobility does not change much with cooling or variation of carrier density. In the second case, mobility at cryogenic temperatures is much larger than at room temperature and displays a distinct power-law dependence on mobility $\mu(4\text{ K}) \propto n^{-\alpha}$, with $\alpha \simeq 0.75$.

diffusive thermoelectric response of degenerate electrons $[S = (k_B/e)(\pi^2/3)(T/T_F)]$ [73]. Moreover, the low-temperature slope S/T was found to be in excellent agreement with the magnitude of the Fermi temperature extracted from quantum oscillations. Cain *et al.* documented the evolution of the Seebeck coefficient of $Sr_{1-x}La_xTiO_3$ and found a phonon-drag peak around 25 K [48], which is also present in our data [Fig. 4(b)]. The fact that this peak occurs near the peak temperature of the lattice thermal conductivity [74] supports the interpretation that the peak is caused by phonon drag as originally suggested [48].

Our focus here is the high-temperature regime, well above both the degeneracy temperature and the phonon-drag regime. In this temperature range, the magnitude of Seebeck coefficient is given by Eq. (4), dubbed "the Pisarenko formula" by Ioffe [76] (and many subsequent authors):

$$|S| = \frac{k_B}{e}\left[2 + r + \ln\left(\frac{2}{n\Lambda^3}\right)\right]. \tag{4}$$

We note that an equation identical to this was already derived by Johnson and Lark-Horovitz as the expression for the Seebeck coefficient of nondegenerate electrons in

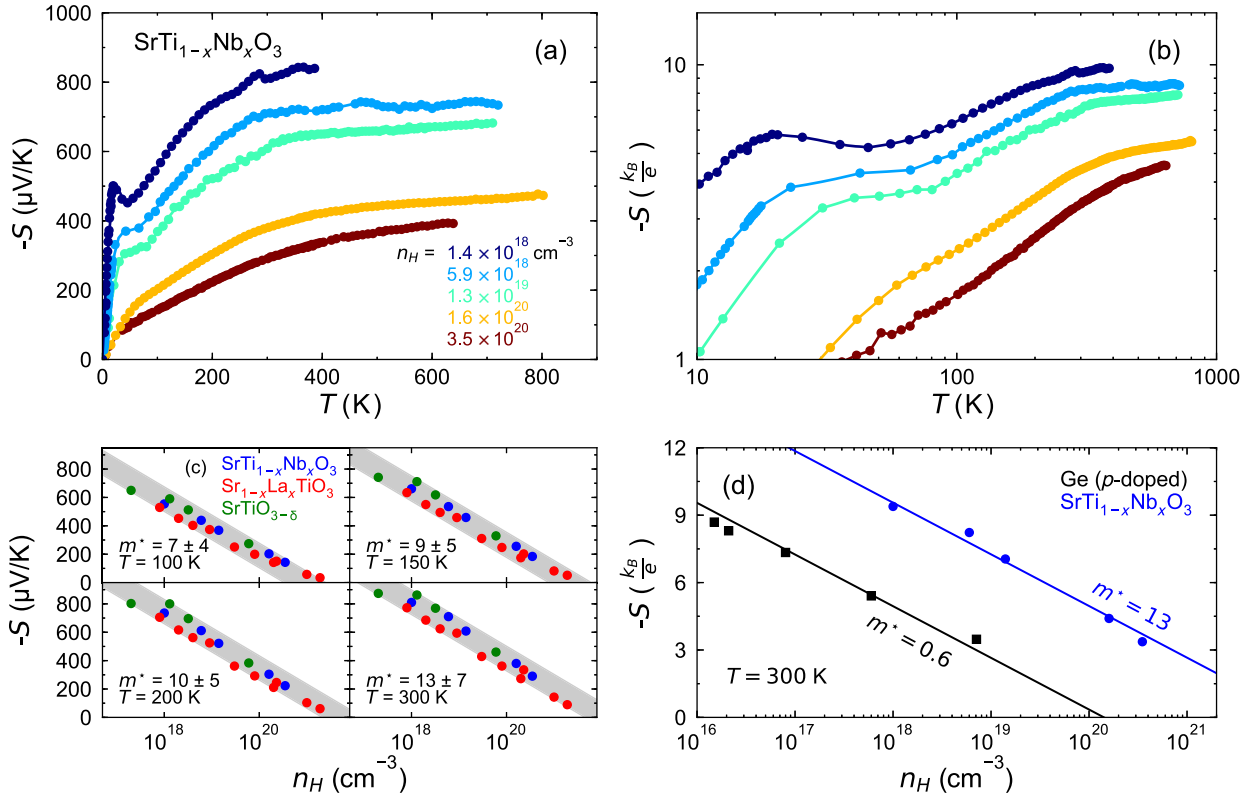

FIG. 4. (a) The Seebeck coefficient as a function of temperature for five Nb-doped $SrTiO_3$ samples from 10 to 800 K. (b) The same data in a log-log plot with S expressed in units of k_B/e. Note the smooth evolution with doping, the presence of a low-temperature phonon-drag peak. In the most dilute sample, the thermoelectric power becomes as large as $10\,k_B/e$, which implies a very large entropy per charge carrier. (c) Variation of the Seebeck coefficient with carrier concentration at different temperatures. Blue circles represent our Nb-doped samples, while green circles represent oxygen-reduced samples [45] and red circles are La-doped samples [48,72]. Thick gray lines represent the behavior expected by Eq. (4). The corresponding effective mass is indicated with an uncertainty set by the width of the line. (d) A comparison of the room-temperature Seebeck coefficient S of p-type Ge [75] and Nb-doped strontium titanate. In both systems S follows a $-\log(n)$ dependence, as expected by Eq. (4). However, at the same carrier concentration, nondegenerate carriers have more entropy in strontium titanate, implying that they are heavier.

germanium crystals [43] when the carrier density is set by extrinsic dopants (and not by thermal excitation of carriers across the band gap). Here, r (also known as the scattering parameter) represents the energy dependence of the scattering time $\tau \propto E^{r-1/2}$, and Λ should be the de Broglie thermal wavelength, $\lambda_{\mathrm{dB}} = \sqrt{(2\pi\hbar^2/m^\star k_B T)}$. When the mean-free path is independent of energy, then $r = 0$, which is what Johnson and Lark-Horovitz [43] assumed in the case of germanium [43]. A simple derivation of Eq. (4) is given in Sec. III of the Supplemental Material (SM) [77].

Let us note that there is a shortcut route toward Eq. (4) thanks to thermodynamics. There is indeed a fundamental link between Eq. (4) and the Sackur-Tetrode [78–80] entropy $\mathcal{S}_{\mathrm{ST}}$ of a monoatomic ideal gas of N atoms [81]:

$$\mathcal{S}_{\mathrm{ST}} = N k_B \left[\frac{5}{2} + \ln\left(\frac{1}{n\lambda_{\mathrm{dB}}^3}\right)\right]. \tag{5}$$

As early as 1948, Callen [82] demonstrated that the Kelvin relation, which can be derived from Onsager reciprocity, implies that the Seebeck coefficient (when it is purely diffusive and not affected by phonon drag) is the ratio of entropy per mobile charge [73,82]. It is not surprising, therefore, to see that Eq. (4) (with $r = 0.5$, which implies a constant scattering time, and an additional factor of 2 due to spin degeneracy) represents the entropy of nondegenerate electrons according to Eq. (5) per charge carrier.

Above degeneracy temperature, $n\lambda_{\mathrm{dB}}^3 < 1$ and $\ln(1/n\lambda_{\mathrm{dB}}^3)$ is positive. It quantifies the temperature-dependent entropy of a perfect gas of indiscernible particles when the primitive cell of the phase space is the Planck constant [81]. With increasing temperature, λ_{dB} shrinks and the number of configurations (for a fixed density of particles) enhances. The heavier the particles, the larger the entropy of the classical gas at a given temperature. This means that the room-temperature entropy of Ar is larger than the room-temperature entropy of Ne [83]. In our context of investigation, the same line of reasoning would imply that the heavier nondegenerate electrons, the larger their Seebeck coefficient.

The relevance of Eq. (4) to our data can be seen by plotting the magnitude of the measured Seebeck coefficient at a given temperature as a function of $\ln(n)$. As seen in Fig. 4(c), at four different temperatures, our data (in blue) combined with what was reported by previous authors for oxygen-reduced [45] (in green) and La-doped [48,72] (in red) strontium titanate correspond to what is expected according to Eq. (4), with $r = 0.5$ and $\Lambda = \lambda_{\mathrm{dB}}$. The extracted effective mass is $7m_e$ at 100 K and rises to $13m_e$ at 300 K.

It is instructive to compare the magnitude of the Seebeck coefficient in our system with a common semiconductor such as germanium. As seen in Fig. 4(d), at room temperature, the Seebeck coefficient in Ge as well as in Nb-doped strontium titanate is a linear function of $\ln(n)$. The two lines have identical slopes but are shifted, implying heavier ($13m_e$ in strontium titanate) and lighter ($0.5m_e$ in Ge) carriers.

E. Temperature dependence of Λ and $m^\star$

Figure 5(a) shows the temperature dependence of Λ, extracted from the Seebeck coefficient combined with Eq. (4) and assuming $r = 0.5$. If Λ is indeed the thermal de Broglie wavelength, its temperature dependence, faster than $T^{-0.5}$ below room temperature, would imply an increasing effective mass. The magnitude of Λ would imply a mass between $6m_e$ and $20m_e$ in the entire temperature range and for all five samples.

The effective mass assuming that $\Lambda = \lambda_{\mathrm{dB}}(m^\star)$ is plotted in Fig. 5(c). One can see that the extracted mass varies with temperature and with carrier density. The figure also shows that our estimation of high-temperature effective mass displays a reasonable extrapolation to the low-temperature effective masses obtained from quantum oscillations [28]. Specifically, when $n_H \simeq 1.5 \times 10^{18}$ cm^{-3}, $m^\star \simeq 2m_e$, and when $n_H > 4 \times 10^{18}$ cm^{-3}, it passes to $m^\star \simeq 4m_e$ [28], as a result of nonparabolic band dispersion of the lower band [30]. This is in agreement with our extracted masses at $n_H = 1.4 \times 10^{18}$ cm^{-3} and at $n_H = 5.8 \times 10^{18}$ cm^{-3}. As seen in Fig. 5(d), our data are also consistent with the $m^\star = 7m_e$ obtained at 150 K from angle-resolved photoemission spectroscopy (ARPES) measurement [84]. Note also the nonmonotonous evolution of the temperature dependence of $m^\star$ as well as the fact that above 500 K, within experimental margin, $m^\star \simeq 10m_e$.

The reported specific heat data at different doping concentrations and different temperature ranges find a low-temperature mass between $1.8m_e$ and $4m_e$ [85]. An excellent agreement between specific heat data at optimal doping [19] and quantum oscillation data [28] can be obtained [86] if one assumes that at optimal doping, the lower band is heavier ($m_1 = 3.85 \pm 0.35m_e$) compared to the higher bands ($m_{2,3} = 1.52 \pm 0.25m_e$). This is in agreement with what is expected by density-functional theory calculations [30] and with the magnitude of the measured superconducting penetration depth [86]. As seen above, these values are also in agreement with our extrapolation to lower temperature.

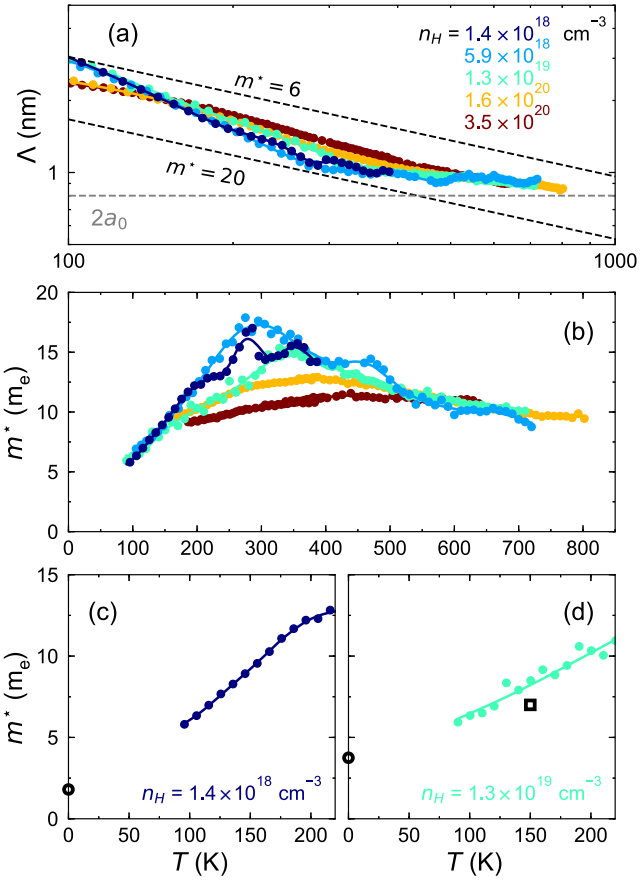

FIG. 5. (a) Temperature dependency of Λ deduced from Eq. (4) using the measured Seebeck coefficient [Fig 4(a)] and assuming $r = 0.5$. Dashed lines represent the temperature dependence for $\lambda_{\mathrm{dB}}(m^\star = 6m_e)$ and $\lambda_{\mathrm{dB}}(m^\star = 20m_e)$. One can see that the data for all temperatures and carrier densities fall between these two lines. (b) Temperature dependence of the effective mass by assuming $\Lambda = \lambda_{\mathrm{dB}}$. Note the nonmonotonous temperature dependence of $m^\star$ and the convergence to a value close to $10m_e$ at high temperature. (c) The effective mass obtained here compared to the low-temperature effective mass obtained by quantum oscillation below 2 K [28] (open circle) at $n_H \simeq 1.4 \times 10^{18}$ cm^{-3}. (d) The effective mass obtained here compared to the low-temperature effective mass obtained by quantum oscillation below 2 K [28] (open circle) and by ARPES at 150 [84] (open square) at $n_H \simeq 1.3 \times 10^{19}$ cm^{-3}.

Note that since the thermal derivative of the entropy of a classical gas does not depend on the mass of the particles, specific heat cannot be used to extract the mass of electrons above the degeneracy temperature. As one can see in Fig. 3 of Ref. [83], in heavier classical gas, entropy is larger, but its thermal slope is the same.

F. Temperature dependence of the Bohr radius

Figure 6(a) shows the temperature dependence of the frequency of the transverse optical phonon, at the center of

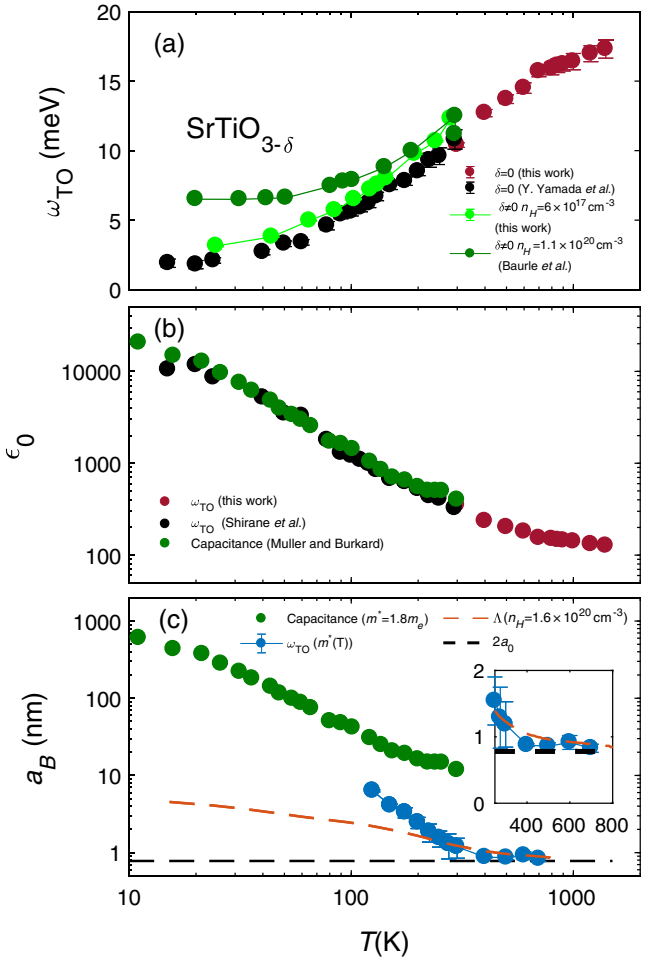

FIG. 6. (a) Temperature dependence of the energy of the soft transverse optical phonon at the zone center extended to 1500 K in insulating $SrTiO_3$ (black and dark red circles) compared to doped $SrTiO_{3-\delta}$ with a carrier density $n_H = 6 \times 10^{17}$ cm^{-3} (light green circles) and $n_H = 1.1 \times 10^{20}$ cm^{-3} (dark green circles) [87]. (b) Temperature dependence of the static electric permittivity ϵ extracted from the energy of the soft mode (black and dark red circles) compared to what was directly measured [4] (dark green circles). (c) The effective Bohr radius, combining the temperature-dependent mass extracted from the Seebeck coefficient and the permittivity quantified by neutron scattering data (dark blue) and the de Broglie thermal wavelength extracted from the Seebeck coefficient Λ (red dashed line). Also shown is a_B with the low-temperature mass (green circles) neglecting its thermal evolution. As highlighted in the inset, a_B saturates above 400 K to twice the lattice parameter (represented by a dashed horizontal line).

the Brillouin zone, up to 1500 K obtained from our neutron scattering measurements. Previously, these soft phonons were extensively studied below room temperature by neutron scattering [87,88], hyper-Raman spectroscopy [89], and optical spectroscopy [6,7,90]. Our new data, in good agreement with early measurements, show that the frequency of this mode, which increases from 1–2 meV at 2 K to 11 meV at 300 K [88,89], continues to rise upon warming above room temperature. The figure also shows how the frequency of the soft mode is affected by doping. Above 200 K, $\omega_{\mathrm{TO}}(T)$ becomes independent of the doping at least up to $n_H = 1.1 \times 10^{20}$ cm^{-3}.

In an ionic solid, the static electric permittivity ϵ_0 and its high-frequency counterpart ϵ_∞ are linked to the longitudinal and transverse frequencies through the Lyddane-Sachs-Teller relation. When there are multiple longitudinal and transverse optical modes, as in our case, one has [91]

$$\prod_{i=1}^{3} \frac{\omega_{\mathrm{LO},i}^2}{\omega_{\mathrm{TO},i}^2} = \frac{\epsilon_0}{\epsilon_\infty}. \tag{6}$$

Assuming that ϵ_∞ and all other optical modes, other than the soft TO1 phonons, do not vary with temperature, this expression implies that $\omega_{\mathrm{TO},1} \propto \sqrt{1/\epsilon_0}$ and the magnitude and the temperature dependence of one can be used to track the evolution of the other. Yamada and Shirane [88] demonstrated that this is indeed the case and $\omega_{\mathrm{TO}} \simeq 194.4/\sqrt{\epsilon_0}$, as one can see in Fig. 6(b). As discussed in SM [77], this prefactor is in excellent agreement with the measured values of longitudinal and transverse phonons. We can therefore safely use our data to track the evolution of ϵ_0 above room temperature.

Our data imply that even at a temperature as high as 1500 K, the electric permittivity is 2 orders of magnitude larger than the vacuum electric permittivity. Nevertheless, compared to its magnitude at 2 K, ϵ_0 has dropped by a factor of 200. Combined with the enhancement in $m^\star(T)$, this leads to drastic shrinking in the Bohr radius, as illustrated in Fig. 6(c). Above 400 K, a_B stops its decrease and saturates to a value of 0.8 nm, almost twice the lattice parameter. Interestingly, this is also the magnitude of Λ in this temperature range [see Fig. 5(a)].

G. Back to the Mott-Ioffe-Regel limit and Planckian dissipation

Having extracted the temperature dependence of $m^\star$, we can return to our resistivity data and compute the mean-free path and the scattering time in this temperature range taking into account the temperature dependence of $m^\star(T)$. As one can see in Fig. 7, both Plankian and MIR limits are verified up to temperatures exceeding room temperature but not above 500 K.

Thus, below 500 K, metallicity of strontium titanate is partially driven by thermal mass amplification. Nevertheless, the mean-free path remains longer than the interactomic distance and the scattering time exceeds the Planckian time. This is no longer the case above 500 K, i.e., when the thermal wavelength saturates to twice the lattice parameter.

In the nondegenerate regime, the electron velocity is set by the thermal energy: $v_{\mathrm{th}} = \sqrt{2k_BT/m^\star}$. Therefore, the inequality $\ell < \Lambda$ is strictly equivalent to the inequality $\tau < \tau_p$ (and vice versa) and a scattering time below the Planckian time means a mean-free path shorter than the

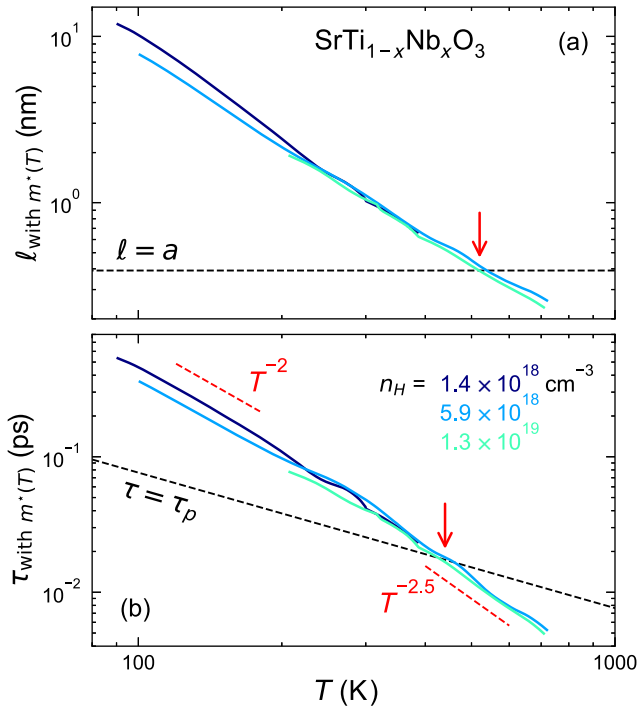

FIG. 7. Temperature dependence of the mean-free path (a) and of the scattering time (b) for the three most dilute samples deduced from the resistivity data and the temperature-dependent effective mass obtained from the Seebeck data. With such a temperature-dependent mass, the mean-free path remains longer than the lattice parameter for $T < 520$ K and the scattering time is longer than the Planckian time for $T < 450$ K. Both limits are violated at higher temperatures.

electronic wavelength. The validity of the scattering-based picture in this context becomes questionable.

III. DISCUSSION

A. Mass amplification and its implications

We saw that our Seebeck data point to a temperature-dependent effective mass. How solid is this conclusion? Can one explain the excess of entropy by a strong energy dependence of the scattering? The answer appears to be negative. Such a route would require an implausibly large r in Eq. (4), as discussed in the Supplemental Material (see Sec. IV of Ref. [77]). There is no independent way to quantify r and ensure that it does not evolve at all with temperature and doping. However, two independent experimental observations establish that r is well below unity and does not evolve with doping. The first is the fact that the Seebeck coefficient at a given temperature is linear in $\ln(n)$, which would have not been the case if r depended on carrier concentration. The second is the fact that above 100 K, mobility at a given temperature shows little or no change with carrier concentration over a very wide window. This implies that the scattering time divided by mass (or alternatively the mean-free path times the wavelength) is not affected by a shift in the chemical potential. The effective mass has been extracted assuming that r is constant and equal to 0.5, which corresponds to assuming that the scattering time does not depend on carrier concentration. This may not be rigorously true. However, a small change in r would not affect our conclusion that the effective mass is of the order of $10m_e$ at room temperature and above (see SM [77] Sec. IV for further details).

This unavoidable heaviness of electrons begs a comment. In intermetallic solids with f electrons, heavy quasiparticles are formed upon cooling. This has been extensively documented during the past three decades. In this case, the quasiparticle mass is boosted by accumulation of entropy due to Kondo coupling between localized spin and the Fermi sea [92]. These are degenerate electrons and the heaviness shows itself in the reciprocal space, where electrons have a Fermi momentum set by the density of carriers. This momentum becomes rapidly fuzzy with warming, leading to large cyclotron masses extracted from temperature dependence of quantum oscillations [93]. The electron heaviness encountered here implies a process occurring in real space. Nondegenerate electrons have a well-defined position and their momentum is thermal. Warming sharpens this position. A large mass means that the thermal sharpening of this position in real space is unusually fast. Note that in both cases, the mass is an entropy-driven process distinct from the band mass associated with momentum-energy dispersion at a fixed temperature (see Fig. 8).

Thus, our conclusion implies a hitherto unknown type of metallicity in a doped polar semiconductor where nondegenerate electrons display a metallic resistivity partially driven by the change in their mass and not merely because of the change in the scattering time. Let us now recall that a temperature-dependent effective mass driven by polaronic effects has been previously suggested in this system.

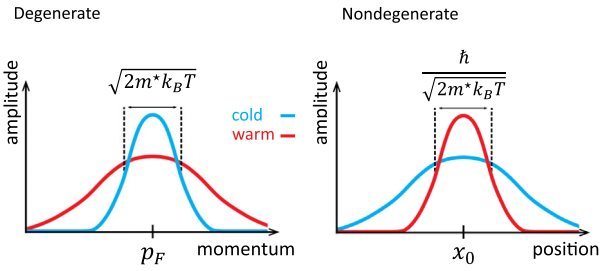

FIG. 8. Left: In the case of degenerate electrons, heaviness refers to the thermal fuzziness of the Fermi momentum. The heavier the electron, the faster the thermal evolution of the sharpness of the amplitude of its wave functions in the reciprocal space. Right: In the case of nondegenerate electrons, heaviness refers to the thermal fuzziness of the position. The heavier the electron, the faster the thermal evolution of the sharpness of the amplitude of its wave functions in the real space.

B. Polarons

At low temperature, there is a large difference between the static and high frequency of electric permittivity. This makes our system a natural platform for emergence of polarons. The nature of polarons in $SrTiO_3$ has been the subject of numerous theoretical discussions. According to Devreese *et al.* [94], the optical conductivity data in $SrTi_{1-x}Nb_xO_3$ can be explained in terms of a gas of large polarons from low to room temperature with no adjustable parameters using a Fröhlich-type interaction with a Frölich-coupling constant $\alpha \simeq 2$. This appeared to provide a satisfactory explanation to the less than threefold mass enhancement seen at low temperatures. Indeed, while the expected band mass is $0.7m_e$ [30], the experimentally observed mass was $1.8m_e$ [12,90]. Note that in this "large polaron" picture, no mass enhancement is expected with rising temperature, because α decreases slightly with rising temperature.

Many years ago, Eagles argued that the electron mass in doped strontium titanate increases with rising temperature based on the magnitude of the plasma frequency quantified by infrared conductivity measurements [95]. He interpreted the data using a theory of mixed polarons [96,97], where the electronic ground state consists of nearly small polarons and weak-coupling large polarons. In this theory, first applied to Zr-doped $SrTiO_3$ at low temperature [96] and later to $SrTi_{1-x}Nb_xO_3$ at high temperature [96,97], the mass enhancement is caused by a change in the electronic overlap integrals or by an increase of the electron-phonon interaction which would increase the contribution of small polarons to the ground state. In the Supplemental Material (see Sec. II of Ref. [77]), we present a short summary of available reports on the evolution of the plasma frequency by different groups.

However, the physical basis for such a change in microscopic parameters remains unclear. Indeed, Ciuchi *et al.* [98] demonstrated that the radius and the mass of Frölich-type polarons both decrease with increasing temperature for a large range of coupling constant values. In the words of Fredrikse *et al.* [45], the polaron ends up "undressing" with warming in any polaronic picture. Therefore, a quantitative account of temperature-induced mass amplification in a polaron-based picture is missing. Taken at its face value, this implies that the polarons are "dressing up" with warming (instead of "dressing down").

C. Metallicity above 500 K

We saw that above room temperature, the effective mass ceases to increase, because Λ, from which it is extracted, saturates above 500 K. In this regime, even with the amplified mass, the mean-free path of charge carriers is below the distance between neighboring atoms and shorter than the wavelength of electrons. This is a challenge for any transport picture based on quasiparticle scattering. In this temperature range, the Bohr radius also saturates, such that $a_B \simeq \Lambda \simeq 2a_0$ (see Fig. 9). Nevertheless, the extracted mean-free path continues to shrink and as a consequence metallicity persists.

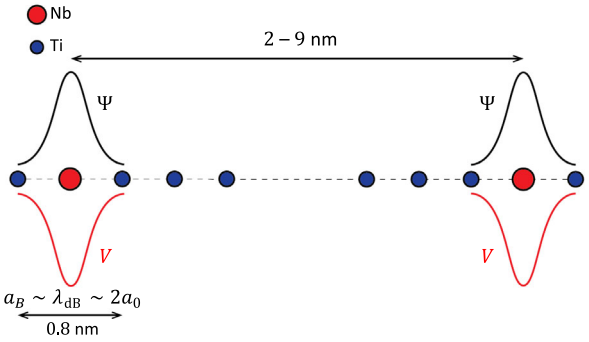

FIG. 9. A sketch of electron wave function and the electrostatic potential dug by substituting Ti with Nb. Above 500 K, the Bohr radius and the de Broglie wavelength both shrink to twice the lattice parameter (0.8 nm). The interdopant distance is significantly longer. Yet, a finite metallic conductivity survives.

The finite conductivity and its decrease with warming can be formulated in Landauer's picture of conduction viewed as transmission [99]. One can state that along "wires" connecting adjacent dopant sites transmission remains finite, but smoothly decreases with warming. In such a picture, there is no need to invoke quasiparticles and their scattering before their proper formation.

The expression for the Seebeck coefficient used to extract the effective mass assumes a classical gas where particle permutation is allowed. Therefore, electrons are not immobilized at the dopant sites. They are strongly coupled to phonons. As seen in Fig. 7, the scattering time follows $T^{-2.5}$ near 500 K. Let us recall that in a conventional picture of electron-phonon scattering, when nondegenerate electrons are scattered by phonons above their Debye temperature the expected behavior for scattering time is $T^{-1.5}$. To sum up, the sheer magnitude of the mean-free path is problematic in a scattering-based picture and its temperature dependence is faster than what would have been expected in a familiar context.

It is instructive to compare the thermal energy of electrons and the depth of the Coulomb potential well. At 500 K, $\epsilon_0 = 150$ and $\epsilon_\infty = 6$. The dynamic and the static Coulomb energy at a Bohr radius are, respectively, $V_0 = 4.5$ meV and $V_\infty = 102$ meV. The kinetic energy at 500 K (43 meV) exceeds V_0, which is low thanks to the screening provided by soft phonons. However, the timescale for thermal electrons ($\hbar/k_BT$) is shorter than the timescale for soft phonons [$\hbar/\omega_0(T)$] when T ~ 500 K and, therefore, this screening may be too slow for faster electrons. A proper treatment of this issue requires proper documentation of the frequency and the wave-vector dependence of the electric permittivity.

IV. SUMMARY

In this paper, we present extended measurements of resistivity and the Seebeck coefficient of Nb-doped strontium titanate to very high temperatures. We started by showing that if one assumes a temperature-independent effective mass, then the very low magnitude of the mobility implies a mean-free path and a scattering time too short compared with the lowest plausible values. We then showed that the magnitude, the doping dependence, and the thermal evolution of the Seebeck coefficient imply a revision of the mean-free path and scattering time. The extracted effective mass extrapolates smoothly to the mass obtained at 2 K by quantum oscillations and at 150 K by ARPES [84]. Injecting this temperature-dependent effective mass to the analysis of resistivity allows us to correct our estimation of the mean-free path and of the scattering time finding that both the MIR and the Planckian limit are respected at room temperature, but not above 500 K.

In the Drude picture, the resistivity of a metal increases with warming, because a fixed number of carriers scatter more frequently with rising temperature. In the case of doped strontium titanate, this picture needs a serious correction, because the enhanced resistivity is partially driven by mass amplification. To the best of our knowledge, there is no microscopic theory for this behavior. However, the similarity between doped strontium titanate and other dilute metals near an aborted ferroelectric order raises the suspicion that such a behavior is intimately connected with the presence of a soft ferrolectric mode.

For temperatures exceeding 500 K, the magnitude of the extracted mass is not sufficiently large to impede the violation of the expected boundaries. Metallicity persists even when the distance between two scattering events is shorter than what is needed to make the existence of a charge carrier meaningful. This is a stark case of metallicity "beyond quasiparticles" [36–38].

V. METHODS

We measured the electric resistivity of six and the Seebeck coefficient of five niobium-doped strontium titanate samples commercially obtained from Crystec with Nb content varying between 0.02 and 2 at.%. The samples had approximate dimensions of $2.5 \times 5 \times 0.5$ mm^3. For all measurements electrical contacts are made with thermal evaporation of gold and 4029 Dupont silver paste. Inelastic neutron scattering experiment have been performed at Orphée reactor. Details are given in the SM (see Sec. V of Ref. [77]).

The resistivity, Hall, and Seebeck measurements from 2 to 400 K were done in a Quantum Design physical property measurement system. The carrier concentration was found to be almost constant between 2 and 300 K, as previously reported. The Seebeck coefficient was measured with an usual "heat on-heat off" technique. One extremity of the sample is glued with silver paint to a copper block that act as a thermal drain, the temperature gradient is applied via a RuO_2 resistor, and the thermal gradient is measured thanks to two type-E thermocouples. The thermal gradient was kept below 10% of the average temperature of the sample.

Electrical resistivity (up to 900 K) and the Seebeck coefficient (up to 800 K) were both measured with a custom-made probe using a 50 W Watlow heater. Sample temperature and thermal gradient were monitored by Pt-100 thermometers directly glued on the sample with 6038 Dupont silver paste. To avoid any additional doping through oxygen reduction, measurements were performed under a rough vacuum of about 10^{-2} mbar, well below what would dope pristine samples. No hysteresis was found upon heating and cooling the sample The data found in the low-temperature and high-temperature sweeps were found to overlap with a reasonable multiplicative factor of the order of 10% due to a difference in the geometrical factor between the two setups.

ACKNOWLEDGMENTS

We thank S. Fratini, A. Georges, S. A. Hartnoll, J. Hemberger, H. Kang, S. A. Kivelson, X. Lin, T. Lorenz, D. Maslov, A. Millis, J. Mravlje, C. W. Rischau, and J. Ruhman for stimulating discussions. We thank M. Delbecq for his help in the early days of this project. This work is supported by the Agence Nationale de la Recherche (ANR-18-CE92-0020-01) and by Jeunes Equipes de l'Institut de Physique du Collège de France.

[1] N. F. Mott, *On the Transition to Metallic Conduction in Semiconductors*, Can. J. Phys. **34**, 1356 (1956).
[2] P. P. Edwards and M. J. Sienko, *Universality Aspects of the Metal-Nonmetal Transition in Condensed Media*, Phys. Rev. B **17**, 2575 (1978).
[3] N. F. Mott, *Metal-Insulator Transitions*, 2nd ed. (Taylor & Francis, London, 1990).
[4] K. A. Müller and H. Burkard, $SrTiO_3$*: An Intrinsic Quantum Paraelectric below 4 K*, Phys. Rev. B **19**, 3593 (1979).
[5] J. Hemberger, P. Lunkenheimer, R. Viana, R. Böhmer, and A. Loidl, *Electric-Field-Dependent Dielectric Constant and Nonlinear Susceptibility in* $SrTiO_3$, Phys. Rev. B **52**, 13159 (1995).
[6] A. A. Sirenko, C. Bernhard, A. Golnik, A. M. Clark, J. Hao, W. Si, and X. X. Xi, *Soft-Mode Hardening in* $SrTiO_3$ *Thin Films*, Nature (London) **404**, 373 (2000).
[7] M. Rössle, C. N. Wang, P. Marsik, M. Yazdi-Rizi, K. W. Kim, A. Dubroka, I. Marozau, C. W. Schneider, J. Humlíček, D. Baeriswyl, and C. Bernhard, *Optical Probe of Ferroelectric Order in Bulk and Thin-Film Perovskite Titanates*, Phys. Rev. B **88**, 104110 (2013).
[8] K. Behnia, *On Mobility of Electrons in a Shallow Fermi Sea over a Rough Seafloor*, J. Phys. Condens. Matter **27**, 375501 (2015).

[9] A. Spinelli, M. A. Torija, C. Liu, C. Jan, and C. Leighton, *Electronic Transport in Doped* $SrTiO_3$*: Conduction Mechanisms and Potential Applications*, Phys. Rev. B **81**, 155110 (2010).

[10] C. Collignon, X. Lin, C. W. Rischau, B. Fauqué, and K. Behnia, *Metallicity and Superconductivity in Doped Strontium Titanate*, Annu. Rev. Condens. Matter Phys. **10**, 25 (2019).

[11] M. N. Gastiasoro, J. Ruhman, and R. M. Fernandes, *Superconductivity in Dilute* $SrTiO_3$*: A Review*, Ann. Phys. (Amsterdam) **417**, 168107 (2020).

[12] X. Lin, Z. Zhu, B. Fauqué, and K. Behnia, *Fermi Surface of the Most Dilute Superconductor*, Phys. Rev. X **3**, 021002 (2013).

[13] J. M. Edge, Y. Kedem, U. Aschauer, N. A. Spaldin, and A. V. Balatsky, *Quantum Critical Origin of the Superconducting Dome in* $SrTiO_3$, Phys. Rev. Lett. **115**, 247002 (2015).

[14] J. Ruhman and P. A. Lee, *Superconductivity at Very Low Density: The Case of Strontium Titanate*, Phys. Rev. B **94**, 224515 (2016).

[15] L. P. Gorkov, *Phonon Mechanism in the Most Dilute Superconductor n-Type* $SrTiO_3$, Proc. Natl. Acad. Sci. U.S.A. **113**, 4646 (2016).

[16] P. Wölfle and A. V. Balatsky, *Superconductivity at Low Density Near a Ferroelectric Quantum Critical Point: Doped* $SrTiO_3$, Phys. Rev. B **98**, 104505 (2018).

[17] D. van der Marel, F. Barantani, and C. W. Rischau, *Possible Mechanism for Superconductivity in Doped* $SrTiO_3$, Phys. Rev. Research **1**, 013003 (2019).

[18] S. N. Klimin, J. Tempere, J. T. Devreese, J. He, C. Franchini, and G. Kresse, *Superconductivity in* $SrTiO_3$*: Dielectric Function Method for Non-Parabolic Bands*, J. Supercond. Novel Magn. **32**, 2739 (2019).

[19] X. Lin, A. Gourgout, G. Bridoux, F. Jomard, A. Pourret, B. Fauqué, D. Aoki, and K. Behnia, *Multiple Nodeless Superconducting Gaps in Optimally Doped* $SrTi_{1-x}Nb_xO_3$, Phys. Rev. B **90**, 140508(R) (2014).

[20] X. Lin, C. W. Rischau, C. J. van der Beek, B. Fauqué, and K. Behnia, *s-Wave Superconductivity in Optimally Doped* $SrTi_{1-x}Nb_xO_3$ Unveiled by Electron Irradiation, Phys. Rev. B **92**, 174504 (2015).

[21] S. E. Rowley, L. J. Spalek, R. P. Smith, M. P. M. Dean, M. Itoh, J. F. Scott, G. G. Lonzarich, and S. S. Saxena, *Ferroelectric Quantum Criticality*, Nat. Phys. **10**, 367 (2014).

[22] A. Stucky, G. W. Scheerer, Z. Ren, D. Jaccard, J.-M. Poumirol, C. Barreteau, E. Giannini, and D. v. d. Marel, *Isotope Effect in Superconducting n-Doped* $SrTiO_3$, Sci. Rep. **6**, 37582 (2016).

[23] C. W. Rischau, X. Lin, C. P. Grams, D. Finck, S. Harms, J. Engelmayer, T. Lorenz, Y. Gallais, B. Fauqué, J. Hemberger, and K. Behnia, *A Ferroelectric Quantum Phase Transition inside the Superconducting Dome of* $Sr_{1-x}Ca_xTiO_{3-\delta}$, Nat. Phys. **13**, 643 (2017).

[24] Y. Tomioka, N. Shirakawa, K. Shibuya, and I. H. Inoue, *Enhanced Superconductivity Close to a Non-Magnetic Quantum Critical Point in Electron-Doped Strontium Titanate*, Nat. Commun. **10**, 738 (2019).

[25] K. Ahadi, L. Galletti, Y. Li, S. Salmani-Rezaie, W. Wu, and S. Stemmer, *Enhancing Superconductivity in* $SrTiO_3$ *Films with Strain*, Sci. Adv. **5**, eaaw0120 (2019).

[26] C. Herrera, J. Cerbin, A. Jayakody, K. Dunnett, A. V. Balatsky, and I. Sochnikov, *Strain-Engineered Interaction of Quantum Polar and Superconducting Phases*, Phys. Rev. Mater. **3**, 124801 (2019).

[27] S. J. Allen, B. Jalan, S. B. Lee, D. G. Ouellette, G. Khalsa, J. Jaroszynski, S. Stemmer, and A. H. MacDonald, *Conduction-Band Edge and Shubnikov–de Haas Effect in Low-Electron-Density* $SrTiO_3$, Phys. Rev. B **88**, 045114 (2013).

[28] X. Lin, G. Bridoux, A. Gourgout, G. Seyfarth, S. Krämer, M. Nardone, B. Fauqué, and K. Behnia, *Critical Doping for the Onset of a Two-Band Superconducting Ground State in* $SrTiO_{3-\delta}$, Phys. Rev. Lett. **112**, 207002 (2014).

[29] A. Bhattacharya, B. Skinner, G. Khalsa, and A. V. Suslov, *Spatially Inhomogeneous Electron State Deep in the Extreme Quantum Limit of Strontium Titanate*, Nat. Commun. **7**, 12974 (2016).

[30] D. van der Marel, J. L. M. van Mechelen, and I. I. Mazin, *Common Fermi-Liquid Origin of* T^2 *Resistivity and Superconductivity in n-Type* $SrTiO_3$, Phys. Rev. B **84**, 205111 (2011).

[31] Y. Tokura, Y. Taguchi, Y. Okada, Y. Fujishima, T. Arima, K. Kumagai, and Y. Iye, *Filling Dependence of Electronic Properties on the Verge of Metal–Mott-Insulator Transition in* $Sr_{1-x}La_xTiO_3$, Phys. Rev. Lett. **70**, 2126 (1993).

[32] X. Lin, B. Fauqué, and K. Behnia, *Scalable* T^2 *Resistivity in a Small Single-Component Fermi Surface*, Science **349**, 945 (2015).

[33] E. Mikheev, B. Himmetoglu, A. P. Kajdos, P. Moetakef, T. A. Cain, C. G. Van de Walle, and S. Stemmer, *Limitations to the Room Temperature Mobility of Two- and Three-Dimensional Electron Liquids in* $SrTiO_3$, Appl. Phys. Lett. **106**, 062102 (2015).

[34] E. Mikheev, S. Raghavan, J. Y. Zhang, P. B. Marshall, A. P. Kajdos, L. Balents, and S. Stemmer, *Carrier Density Independent Scattering Rate in* $SrTiO_3$*-Based Electron Liquids*, Sci. Rep. **6**, 20865 (2016).

[35] J. Wang, L. Yang, C. W. Rischau, Z. Xu, Z. Ren, T. Lorenz, J. Hemberger, X. Lin, and K. Behnia, *Charge Transport in a Polar Metal*, npj Quantum Mater. **4**, 61 (2019).

[36] X. Lin, C. W. Rischau, L. Buchauer, A. Jaoui, B. Fauqué, and K. Behnia, *Metallicity Without Quasi-Particles in Room-Temperature Strontium Titanate*, npj Quantum Mater. **2**, 41 (2017).

[37] A. S. Mishchenko, L. Pollet, N. V. Prokof'ev, A. Kumar, D. L. Maslov, and N. Nagaosa, *Polaron Mobility in the "Beyond Quasiparticles" Regime*, Phys. Rev. Lett. **123**, 076601 (2019).

[38] J.-J. Zhou and M. Bernardi, *Predicting Charge Transport in the Presence of Polarons: The Beyond-Quasiparticle Regime in* $SrTiO_3$, Phys. Rev. Research **1**, 033138 (2019).

[39] O. Gunnarsson, M. Calandra, and J. E. Han, *Colloquium: Saturation of Electrical Resistivity*, Rev. Mod. Phys. **75**, 1085 (2003).

[40] S. Fratini, D. Mayou, and S. Ciuchi, *The Transient Localization Scenario for Charge Transport in Crystalline Organic Materials*, Adv. Funct. Mater. **26**, 2292 (2016).

[41] B. Shklovskii and A. Efros, *Electronic Properties of Doped Semiconductors* (Springer, Berlin, 1984).
[42] J. Bruin, H. Sakai, R. Perry, and A. Mackenzie, *Similarity of Scattering Rates in Metals Showing T-Linear Resistivity*, Science **339**, 804 (2013).
[43] V. A. Johnson and K. Lark-Horovitz, *Theory of Thermoelectric Power in Semiconductors with Applications to Germanium*, Phys. Rev. **92**, 226 (1953).
[44] D. M. Eagles, M. Georgiev, and P. C. Petrova, *Explanation for the Temperature Dependence of Plasma Frequencies in* $SrTiO_3$ *Using Mixed-Polaron Theory*, Phys. Rev. B **54**, 22 (1996).
[45] H. P. R. Frederikse, W. R. Thurber, and W. R. Hosler, *Electronic Transport in Strontium Titanate*, Phys. Rev. **134**, A442 (1964).
[46] H. P. R. Frederikse and W. R. Hosler, *Hall Mobility in* $SrTiO_3$, Phys. Rev. **161**, 822 (1967).
[47] O. N. Tufte and P. W. Chapman, *Electron Mobility in Semiconducting Strontium Titanate*, Phys. Rev. **155**, 796 (1967).
[48] T. A. Cain, A. P. Kajdos, and S. Stemmer, *La-Doped* $SrTiO_3$ *Films with Large Cryogenic Thermoelectric Power Factors*, Appl. Phys. Lett. **102**, 182101 (2013).
[49] C. Yamanouchi, K. Mizuguchi, and W. Sasaki, *Electric Conduction in Phosphorus Doped Silicon at Low Temperatures*, J. Phys. Soc. Jpn. **22**, 859 (1967).
[50] H. Barber, *Effective Mass and Intrinsic Concentration in Silicon*, Solid-State Electron. **10**, 1039 (1967).
[51] J. F. Koch, R. A. Stradling, and A. F. Kip, *Some New Aspects of Cyclotron Resonance in Copper*, Phys. Rev. **133**, A240 (1964).
[52] R. A. Matula, *Electrical Resistivity of Copper, Gold, Palladium, and Silver*, J. Phys. Chem. Ref. Data **8**, 1147 (1979).
[53] R. Settai, H. Shishido, S. Ikeda, Y. Murakawa, M. Nakashima, D. Aoki, Y. Haga, H. Harima, and Y. Onuki, *Quasi-Two-Dimensional Fermi Surfaces and the de Haas–van Alphen Oscillation in Both the Normal and Superconducting Mixed States of* $CeCoIn_5$, J. Phys. Condens. Matter **13**, L627 (2001).
[54] A. McCollam, S. R. Julian, P. M. C. Rourke, D. Aoki, and J. Flouquet, *Anomalous de Haas—van Alphen Oscillations in* $CeCoIn_5$, Phys. Rev. Lett. **94**, 186401 (2005).
[55] M. A. Tanatar, J. Paglione, C. Petrovic, and L. Taillefer, *Anisotropic Violation of the Wiedemann-Franz Law at a Quantum Critical Point*, Science **316**, 1320 (2007).
[56] A. Ioffe and A. Regel, *Non-Crystalline, Amorphous and Liquid Electronic Semiconductors*, Prog. Semicond. **4**, 237 (1960).
[57] N. F. Mott, *Conduction in Non-Crystalline Systems IX. The Minimum Metallic Conductivity*, Philos. Mag. **26**, 1015 (1972).
[58] V. J. Emery and S. A. Kivelson, *Superconductivity in Bad Metals*, Phys. Rev. Lett. **74**, 3253 (1995).
[59] J. Mooij, *Electrical Conduction in Concentrated Disordered Transition Metal Alloys*, Phys. Status Solidi A **17**, 521 (1973).
[60] Z. Fisk and G. W. Webb, *Saturation of the High-Temperature Normal-State Electrical Resistivity of Superconductors*, Phys. Rev. Lett. **36**, 1084 (1976).
[61] O. Gunnarsson, M. Calandra, and J. E. Han, *Colloquium: Saturation of Electrical Resistivity*, Rev. Mod. Phys. **75**, 1085 (2003).
[62] N. Hussey, K. Takenaka, and H. Takagi, *Universality of the Mott-Ioffe-Regel Limit in Metals*, Philos. Mag. **84**, 2847 (2004).
[63] S. A. Hartnoll, *Theory of Universal Incoherent Metallic Transport*, Nat. Phys. **11**, 54 (2015).
[64] A. Legros, S. Benhabib, W. Tabis, F. Lalibert, M. Dion, M. Lizaire, B. Vignolle, D. Vignolles, H. Raffy, Z. Z. Li, P. Auban-Senzier, N. Doiron-Leyraud, P. Fournier, D. Colson, L. Taillefer, and C. Proust, *Universal T-Linear Resistivity and Planckian Dissipation in Overdoped Cuprates*, Nat. Phys. **15**, 142 (2019).
[65] K. Huang, T. Uen, Y. Gou, C. Huang, and H.-C. Yang, *Temperature Dependence of Transport Properties of Evaporated Indium Tin Oxide Films*, Thin Solid Films **148**, 7 (1987).
[66] A. K. Das, P. Misra, R. Ajimsha, A. Bose, S. Joshi, D. Phase, and L. Kukreja, *Studies on Temperature Dependent Semiconductor to Metal Transitions in ZnO Thin Films Sparsely Doped with Al*, J. Appl. Phys. **112**, 103706 (2012).
[67] B. D. Ahn, S. H. Oh, H. J. Kim, M. H. Jung, and Y. G. Ko, *Low Temperature Conduction and Scattering Behavior of Ga-Doped ZnO*, Appl. Phys. Lett. **91**, 252109 (2007).
[68] R. M. Naidu, A. Subrahmanyam, A. Verger, M. Jain, S. B. Rao, S. Jha, and D. Phase, *Electron-Electron Interactions Based Metal-Insulator Transition in Ga Doped ZnO Thin Films*, Electron. Mater. Lett. **8**, 457 (2012).
[69] J. Engelmayer, X. Lin, C. P. Grams, R. German, T. Fröhlich, J. Hemberger, K. Behnia, and T. Lorenz, *Charge Transport in Oxygen-Deficient* $EuTiO_3$: *The Emerging Picture of Dilute Metallicity in Quantum-Paraelectric Perovskite Oxides*, Phys. Rev. Mater. **3**, 051401 (2019).
[70] S. H. Wemple, *Some Transport Properties of Oxygen-Deficient Single-Crystal Potassium Tantalate (*$KTaO_3$*)*, Phys. Rev. **137**, A1575 (1965).
[71] R. S. Allgaier and W. W. Scanlon, *Mobility of Electrons and Holes in PbS, PbSe, and PbTe between Room Temperature and 4.2 K*, Phys. Rev. **111**, 1029 (1958).
[72] T. Okuda, K. Nakanishi, S. Miyasaka, and Y. Tokura, *Large Thermoelectric Response of Metallic Perovskites:* $Sr_{1-x}La_xTiO_3$ $(0 < x < 0.1)$, Phys. Rev. B **63**, 113104 (2001).
[73] K. Behnia, *Fundamentals of Thermoelectricity* (Oxford University Press, Oxford, 2015).
[74] V. Martelli, J. L. Jiménez, M. Continentino, E. Baggio-Saitovitch, and K. Behnia, *Thermal Transport and Phonon Hydrodynamics in Strontium Titanate*, Phys. Rev. Lett. **120**, 125901 (2018).
[75] T. H. Geballe and G. W. Hull, *Seebeck Effect in Germanium*, Phys. Rev. **94**, 1134 (1954).
[76] A. Ioffe, *Semiconductor Thermoelements and Thermoelectric Cooling* (Infosearch Limited, London, 1957).
[77] See Supplemental Material at http://link.aps.org/supplemental/10.1103/PhysRevX.10.031025 for more details on the exponent of the power law in the temperature dependence of the resistivity, a brief discussion of the previously measured plasma frequency, a derivation of the Pisarenko formula, a brief discussion on the scattering

parameter, details on the neutron scattering experiment, and more details on the Lyddane-Sachs-Teller relation and its application to strontium titanate.

[78] O. Sackur, *The Application of the Kinetic Theory of Gases to Chemical Problems*, Ann. Phys. (Berlin) **341**, 958 (1911).

[79] O. Sackur, *Die Bedeutung des elementaren Wirkungsquantums fur die Gastheorie und die Berechnung der chemischen Konstanten*, in *Festschrift W. Nernst zu seinem 25 jährigen Doktorjubiläum* (Verlag Wilhelm Knapp, Halle, 1912), pp. 405–423.

[80] H. von Tetrode, *The Chemical Constant of Gases and the Elementary Quantum of Action*, Ann. Phys. (Berlin) **343**, 434 (1912).

[81] C. Kittel and K. Herbert, *Thermal Physics* (W.H. Freeman and Company, San Francisco, 1980).

[82] H. B. Callen, *The Application of Onsager's Reciprocal Relations to Thermoelectric, Thermomagnetic, and Galvanomagnetic Effects*, Phys. Rev. **73**, 1349 (1948).

[83] J. P. Francisco and E. Pérez, *Sackur-Tetrode Equation in the Lab*, Eur. J. Phys. **36**, 055033 (2015).

[84] Y. J. Chang, A. Bostwick, Y. S. Kim, K. Horn, and E. Rotenberg, *Structure and Correlation Effects in Semiconducting* $SrTiO_3$, Phys. Rev. B **81**, 235109 (2010).

[85] M. Ahrens, R. Merkle, B. Rahmati, and J. Maier, *Effective Masses of Electrons in n-Type* $SrTiO_3$ *Determined from Low-Temperature Specific Heat Capacities*, Physica (Amsterdam) **393B**, 239 (2007).

[86] C. Collignon, B. Fauqué, A. Cavanna, U. Gennser, D. Mailly, and K. Behnia, *Superfluid Density and Carrier Concentration across a Superconducting Dome: The Case of Strontium Titanate*, Phys. Rev. B **96**, 224506 (2017).

[87] D. Bäuerle, D. Wagner, M. Wöhlecke, B. Dorner, and H. Kraxenberger, *Soft Modes in Semiconducting* $SrTiO_3$: II. *The Ferroelectric Mode*, Z. Phys. B **38**, 335 (1980).

[88] Y. Yamada and G. Shirane, *Neutron Scattering and Nature of the Soft Optical Phonon in* $SrTiO_3$, J. Phys. Soc. Jpn. **26**, 396 (1969).

[89] H. Vogt, *Refined Treatment of the Model of Linearly Coupled Anharmonic Oscillators and Its Application to the Temperature Dependence of the Zone-Center Soft-Mode Frequencies of* $KTaO_3$ *and* $SrTiO_3$, Phys. Rev. B **51**, 8046 (1995).

[90] D. van Mechelen, *Charge and Spin Electrodynamics of* $SrTiO_3$ *and* $EuTiO_3$ *Studied by Optical Spectroscopy*, Ph.D. Thesis, Geneva University, 2010.

[91] W. Cochran and R. A. Cowley, *Dielectric Constants and Lattice Vibrations*, J. Phys. Chem. Solids **23**, 447 (1962).

[92] A. C. Hewson, *The Kondo Problem to Heavy Fermions* (Cambridge University Press, Cambridge, England, 1993).

[93] L. Taillefer and G. G. Lonzarich, *Heavy-Fermion Quasiparticles in* UPt_3, Phys. Rev. Lett. **60**, 1570 (1988).

[94] J. T. Devreese, S. N. Klimin, J. L. M. van Mechelen, and D. van der Marel, *Many-Body Large Polaron Optical Conductivity in* $SrTi_{1-x}Nb_xO_3$, Phys. Rev. B **81**, 125119 (2010).

[95] F. Gervais, J.-L. Servoin, A. Baratoff, J. G. Bednorz, and G. Binnig, *Temperature Dependence of Plasmons in Nb-Doped* $SrTiO_3$, Phys. Rev. B **47**, 8187 (1993).

[96] D. M. Eagles, *Adiabatic Theory of Nearly Small Polarons*, Phys. Rev. **145**, 645 (1966).

[97] D. M. Eagles, *Theory of Transitions from Large to Nearly-Small Polarons, with Application to Zr-Doped Superconducting* $SrTiO_3$, Phys. Rev. **181**, 1278 (1969).

[98] S. Ciuchi, J. Lorenzana, and C. Pierleoni, *Induced Charge in a Fröhlich Polaron: Sum Rule and Spatial Extent*, Phys. Rev. B **62**, 4426 (2000).

[99] Y. Imry and R. Landauer, *Conductance Viewed as Transmission*, Rev. Mod. Phys. **71**, S306 (1999).